

Comparison of satellite-derived TOA shortwave clear-sky fluxes to estimates from GCM simulations constrained by satellite observations of land surface characteristics

Valentine G. Anantharaj,^a Udaysankar S. Nair,^{b*} Peter Lawrence,^c Thomas N. Chase,^c
Sundar Christopher^b and Thomas Jones^b

^a Geosystems Research Institute, Mississippi State University, Box 9652, Mississippi State, MS 39762, USA

^b Earth System Scientific Center, National Space Science and Technology Center (NSSTC), 320 Sparkman Drive, Huntsville, AL 35805, USA

^c Cooperative Institute for Research in Environmental Studies, University of Colorado, Boulder, CO 80309, USA

ABSTRACT: Clear-sky, upwelling shortwave flux at the top of the atmosphere ($S_{\text{TOA}}^{\uparrow}$), simulated using the atmospheric and land model components of the Community Climate System Model 3 (CCSM3), is compared to corresponding observational estimates from the Clouds and Earth's Radiant Energy System (CERES) sensor. Improvements resulting from the use of land surface albedo derived from Moderate Resolution Imaging Spectroradiometer (MODIS) to constrain the simulations are also examined. Compared to CERES observations, CCSM3 overestimates global, annual averaged $S_{\text{TOA}}^{\uparrow}$ over both land and oceans. However, regionally, CCSM3 overestimates $S_{\text{TOA}}^{\uparrow}$ over some land and ocean areas while underestimating it over other sites. CCSM3 underestimates $S_{\text{TOA}}^{\uparrow}$ over the Saharan and Arabian Deserts and substantial differences exist between CERES observations and CCSM3 over agricultural areas. Over selected sites, after using ground-based observations to remove systematic biases that exist in CCSM3 computation of $S_{\text{TOA}}^{\uparrow}$, it is found that use of MODIS albedo improves the simulation of $S_{\text{TOA}}^{\uparrow}$. Inability of coarse resolution CCSM3 simulation to resolve spatial heterogeneity of snowfall over high altitude sites such as the Tibetan Plateau causes overestimation of $S_{\text{TOA}}^{\uparrow}$ in these areas. Discrepancies also exist in the simulation of $S_{\text{TOA}}^{\uparrow}$ over ocean areas as CCSM3 does not account for the effect of wind speed on ocean surface albedo. This study shows that the radiative energy budget at the TOA is improved through the use of MODIS albedo in Global Climate Models. Copyright © 2010 Royal Meteorological Society

KEY WORDS radiation energy budget; shortwave fluxes; global circulation model; CERES; MODIS land surface albedo; ocean albedo; vegetation albedo

Received 1 December 2008; Revised 30 December 2009; Accepted 12 January 2010

1. Introduction

Research over the past three decades shows that anthropogenic activities have the potential to significantly impact global and regional climates. One such anthropogenic activity that has received considerable attention in recent years is the increased emission of greenhouse gases, specifically carbon dioxide (CO_2). Increasing concentration of greenhouse gases results in a reduction of net outgoing longwave radiation from the earth–atmosphere system leading to an increase in surface temperatures. Observations show increasing surface temperature trends in recent decades (IPCC, 2007), which has been partly attributed to increasing atmospheric CO_2 concentrations. Identification of increasing CO_2 as the primary cause of warming trends in surface air temperature is based primarily on Global Climate Model (GCM)

simulations. As GCMs are extensively utilised in assessments of climate change, realism of different processes simulated by GCMs is of significant interest.

Analysis of the top of the atmosphere (TOA) radiative energy budget, characterised by an approximate balance between the net incoming solar radiation and outgoing terrestrial longwave radiation, is important in climate change studies. In recent decades, radiative energy budget at the TOA has been monitored using satellite-borne instruments such as the Earth Radiation Budget Experiment (ERBE) and Clouds and Earth's Radiant Energy System (CERES). These satellite sensors provide datasets that allow evaluation of the performance of GCMs from a global energy budget perspective.

Net incoming shortwave radiation at the TOA, the main energy input into the earth–atmosphere system, is modulated by the planetary albedo, which is the proportion of the incoming solar radiation reflected back to space by the land and ocean surface, clouds and atmospheric aerosols. Bender *et al.* (2006) compared planetary albedo from 20 GCMs used in the Fourth Assessment Report (AR4) of the Intergovernmental Panel

* Correspondence to: Udaysankar S. Nair, National Space Science and Technology Center (NSSTC), 3046, Huntsville, AL 35805, USA.
E-mail: nair@nsstc.uah.edu

on Climate Change (IPCC). This comparison found systematic differences between satellite observations and numerical model-simulated values of planetary albedo with the models consistently providing a higher estimate. Comparison of mean planetary albedo from the 20 GCMs to satellite observations shows that the models overestimate the planetary albedo during boreal summer and underestimate it during austral summer.

Studies have also examined the impact of individual factors that contribute to the planetary albedo separately, with a substantial body of the research focussing on the contribution of clouds and aerosols to planetary albedo and the TOA radiation budget (Charlson *et al.*, 1992; Chen *et al.*, 2000; Potter and Cess, 2004). However, there are relatively fewer studies that address the contribution of the land and ocean surface to planetary albedo and the TOA radiation budget. Relevant in this context are the realistic representation of spatiotemporal albedo variations caused by snow, ice and vegetation cover.

Seasonal changes of snow cover result in large gradients of surface albedo in the extra-tropical regions of the Northern Hemisphere (NH), with the spring thawing of snow decreasing the surface albedo. Associated with the melting of snow is the positive feedback effect of decreasing the surface albedo which in turn increases surface air temperature further accelerating the snow melt. This surface albedo feedback effect is important in the context of climate change, with nearly half of the surface air temperature response in doubled CO₂ GCM experiments being attributed to the snow-albedo feedback effect (Hall, 2004). Using an analytical model and satellite observations, Qu and Hall (2006) analyzed and compared a set of 17 GCM simulations from IPCC-AR4, and summarized that in the extra-tropical regions of the NH, the atmosphere attenuates the net impacts due to snow cover anomalies by 50%; and that there was large variability among the AR4 models in translating the changes in the surface air temperatures (SAT) to surface albedo anomalies and thereby snow-albedo feedbacks. Hence, they recommend developing alternate parameterisation to represent snow and land surface processes, a suggestion also noted by Levis *et al.* (2007). Further, systematic positive biases in spring albedo, due to snow cover and the melting of snow later in the spring, have also been found to be prevalent among most of the IPCC-AR4 models evaluated by Roesch (2006).

Nair *et al.* (2007) compared GCM estimates of the TOA radiative forcing over southwest Australia, a region of drastic land-use change in recent decades, against satellite observations. They found significant differences between the GCM estimates and satellite observations and concluded that parameterisations utilised in GCMs may not realistically represent the spatiotemporal variations in land surface characteristics including albedo, especially in regions of agricultural land use where the seasonal variation of albedo is governed by the type of agricultural species and also by land management practices.

1.1. Study objectives and analysis framework

The main objectives of this study were to: (1) examine the validity of the representation of surface albedo in the Community Land Model – Version 3 (CLM3) of the Community Climate System Model 3.0 (CCSM3), one of the GCMs used in IPCC assessments, by comparing it to CERES satellite observations of clear-sky shortwave fluxes at the TOA (referred from here on as $S_{\text{TOA}}^{\uparrow}$); (2) study the impact of using broadband albedos derived from the Moderate Resolution Imaging Spectroradiometer (MODIS) to constrain CLM3 used in CCSM3 on the simulated $S_{\text{TOA}}^{\uparrow}$ values; and (3) examine whether the introduction of an improved land surface parameterisation (in addition to the use of MODIS-derived albedo to constrain CLM3) will improve the simulation of $S_{\text{TOA}}^{\uparrow}$. Note that in the set of experiments used in this study, the CCSM3 was configured to utilise the Community Atmospheric Model 3.0 (CAM3) coupled to the Community Land Model 3.0 (CLM3) of CCSM3 with the bottom boundary conditions over the oceans specified using the climatological sea surface temperatures (SST) and sea ice extent. From this point on, references to CCSM3 simulations are to be understood in the context that only the fully coupled atmosphere and land components (CAM3+CLM3) of CCSM3 have been used and that the dynamic ocean model component of CCSM3 was not utilised in these studies.

Note that the CCSM3 simulation of $S_{\text{TOA}}^{\uparrow}$ is impacted by land surface albedo and column loading of gases that are radiatively active in the shortwave part of the spectrum (mainly water vapour and ozone). Further, land surface albedo is modulated by precipitation with rainfall modifying the bare soil albedo and snow altering albedo of both soil and vegetation. There is also a solar zenith angle (SZA) dependence of the surface albedo, which is not adequately accounted for in many weather and climate models (Wang *et al.*, 2007). Imperfect cloud screening introduces errors in CERES-derived estimates of $S_{\text{TOA}}^{\uparrow}$. Thus understanding the cause for differences between CCSM3-simulated $S_{\text{TOA}}^{\uparrow}$ and CERES-derived estimates is complicated due to multiple dependencies, non-linear interactions between some of the dependent factors and also systematic biases in the radiative transfer parameterisation used in CCSM3. Assessing the impact of MODIS-derived broadband albedo on CCSM3 simulation of $S_{\text{TOA}}^{\uparrow}$ also requires a quantification of errors introduced by multiple dependencies.

Conduct of such a detailed error analysis at the global scale is complicated due to the availability of required datasets and hence is beyond the scope of the present study. However, this study quantifies systematic biases introduced by the radiative transfer parameterisation and by errors in CCSM3 simulation of column water vapour loading over two selected sites where data required for conducting such analysis is available. Results from this limited quantitative analysis will be used to qualitatively interpret CERES–CCSM3 comparisons over other areas.

2. Study area

Comparisons of CCSM3-simulated $S_{\text{TOA}}^{\uparrow}$ and CERES observations are conducted over a global domain. Selected areas over mountainous regions, deserts, tropical forests and agricultural areas are examined in detail. Agricultural areas examined include: (1) the Mississippi Delta region, a site of large-scale irrigated agriculture; (2) southwest Australia, a site of large-scale rain-fed agriculture; (3) rural agricultural areas around Hyderabad, in Andhra Pradesh, India; and (4) a heavily instrumented observational site, maintained as part of the Atmospheric Radiation Measurement (ARM) Program, at the Southern Great Plains-Central Facility (SGP-CF) located in Lamont, OK. In addition to the SGP-CF location, we also use observational data from the ARM Mobile Facility deployed in Niamey, Niger. In the respective areas covered by the CCSM grid cells for the two ARM sites, the two dominant land cover classes are cropland (52%) and grassland (30%) for the SGP-CF and grassland (59%) and bare ground (27%) for the Niger site. Note that use of satellite observations to constrain land surface albedo is expected to significantly impact simulations over areas influenced by anthropogenic activities (Nair *et al.*, 2007). This hypothesis is examined by intercomparing the performance of CCSM3 over agricultural areas to forested regions, which have more predictable phenology patterns better captured by parameterisations in GCMs.

3. Methodology

This study compares GCM climatologies of $S_{\text{TOA}}^{\uparrow}$ from three different GCM experiments to a 7-year climatology of clear-sky $S_{\text{TOA}}^{\uparrow}$ derived from CERES observations from the Terra satellite to evaluate the impact of using satellite-derived albedo to constrain GCMs.

3.1. CCSM3 climate simulation experiments

The three CCSM3 climate simulations (being referred to as 'CONTROL', 'CLM-MODIS' and 'CLM-SiB') utilised T42 grid resolution under current day atmospheric CO_2 concentrations (355 ppm) using prescribed cycling monthly SSTs and sea ice distributions from a climatology of 1950–2003 (Lawrence and Chase, 2007). The simulations were run for a period of 15 years. The simulated $S_{\text{TOA}}^{\uparrow}$ climatology used in this study was constructed from the last 10 years of the simulation with the first 5 years being discarded as the spin up. Relevant details of the three different experiments are given in the following sections.

3.1.1. The CONTROL experiment

The control experiment (referred to as CONTROL) was run with the default CAM3 and CLM3 coupled atmospheric and land model components of CCSM 3.0, as provided by National Center for Atmospheric Research (NCAR). The default version of CCSM3 utilises the CLM3 where land surface characteristics are specified

using the standard NCAR land surface parameters as described in Oleson *et al.* (2004). The description of physical processes and the land surface boundary data are evaluated through climate simulations with the CLM and the CCSM in Bonan *et al.* (2002) and Dickinson *et al.* (2006). The improved physical processes of CLM3 and the representation of land surface boundary conditions had overall helped to improve CCSM3.

3.1.2. The CLM-MODIS experiment

Several studies have addressed the deficiencies in the parameterisation of land surface albedo in the Community Land Model 2.0 by comparing the model-computed albedo against MODIS observations (Oleson *et al.*, 2003; Zhou *et al.*, 2003; Wang *et al.*, 2004). These studies report better agreement of simulated albedo to observations during summer (Oleson *et al.*, 2003), overestimation of simulated albedo over snow-covered regions by as much as 20% and underestimation of the albedo in the desert regions of the Sahara and the Arabian Peninsula (Oleson *et al.*, 2003; Zhou *et al.*, 2003). These studies suggested CLM needs to be improved to have a better representation of albedo, leaf area index (LAI), snow cover etc. in order to better depict the interaction of downwelling solar radiation with the land surface.

The prescription of land surface parameters using MODIS-derived observations has been used to improve the performance of CLM with significant impacts to climate simulations (Tian *et al.*, 2004a, 2004b; Lawrence and Chase, 2007). This approach is used in the second experiment considered in this study, referred to hereon as CLM-MODIS. In the CLM-MODIS experiment, the MODIS vegetation continuous fields data of Hansen *et al.* (2003), along with the land cover mapping of Friedl *et al.* (2002), and the prescribed crop distributions of Ramankutty and Foley (1999) are used to generate current day plant functional type (PFT) distributions. The monthly averaged MODIS LAI data from Myneni *et al.* (2002) and surface albedo from Schaaf *et al.* (2002) are used to prescribe PFT LAI values and soil colour, both of which are used in CLM to calculate the radiation dynamics of vegetation and bare soils. New soil colours are derived by fitting visible and near infrared soil reflectance values for each grid cell and for each month, to make the average monthly snow-free surface albedo in CLM consistent with MODIS observations at local solar noon on the middle day of the month. These soil reflectance values are then adjusted to be further consistent with the model soil moisture climatology so that the soil reflectance for a given soil moisture content is reproduced (Lawrence and Chase, 2007).

Compared to the default CLM3 parameters, the new MODIS-derived parameters increase the bare soil fraction by 10% which is realised through reduced tree, shrub and crop cover. The new parameters also result in average increases of 10% for LAI and stem area index (SAI) values, with the largest increases in tropical forests. Though the vegetated fraction decreased overall (and so

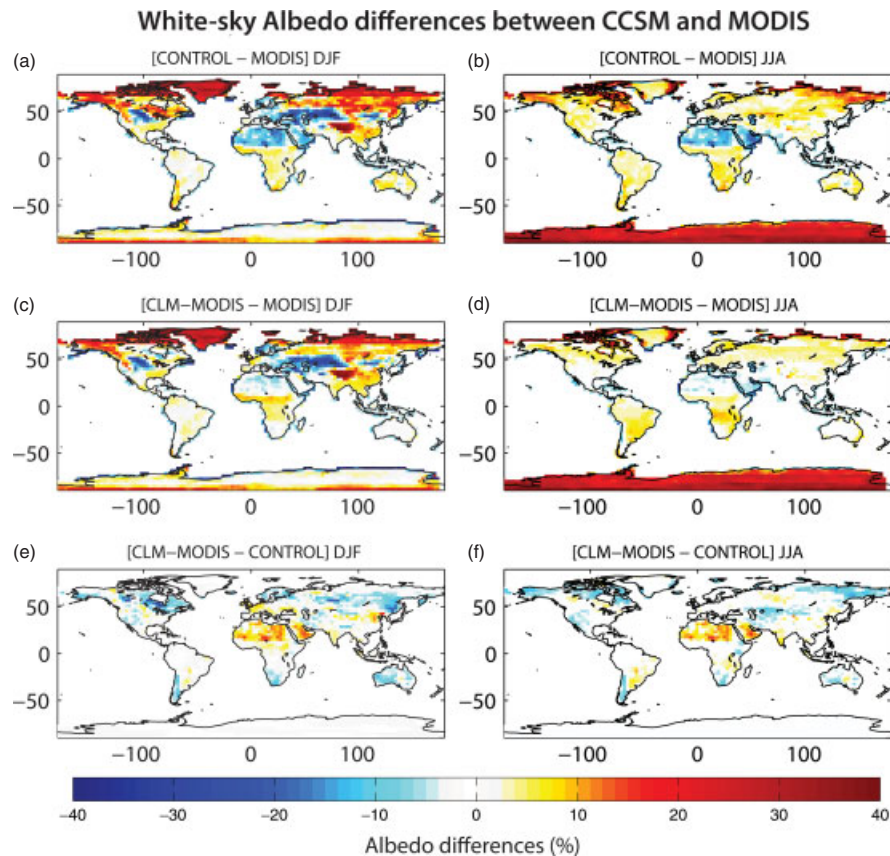


Figure 1. Differences in average seasonal local noon broadband whitesky surface albedo (%) between MODIS and the CONTROL experiment (a and b); with the new MODIS-derived parameters (CLM–MODIS) experiment (c and d) and differences between the CLM–MODIS and CONTROL experiments (e and f). This figure is available in colour online at wileyonlinelibrary.com/journal/joc

bare soil increased), the much larger increase in LAI/SAI in the vegetated fraction more than compensated for the increased bare soil fraction area so that LAI/SAI was on average are larger. The default CLM land parameters resulted in much higher values of albedo across much of NH and in significantly lower values across the Sahara and Arabian deserts (Figure 1(a) and (b)). The new parameters significantly reduced the CLM3 surface albedo for all seasons which reduces the high albedo difference found between the CLM 3.0 and MODIS albedo over all seasons (Figure 1(e) and (f)). The changes in soil colour with the new parameters have the largest impact on albedo in areas with sparse vegetation that are not affected by snow. In general, the new soil colours lowered the effective soil reflectance in densely vegetated regions and increased the soil reflectance in the desert regions.

3.1.3. The CLM–SiB experiment with MODIS land surface parameters

The CLM–SiB experiment uses a new surface hydrology scheme in CLM3 that is consistent with the one used in the Simple Biosphere (SiB 2.0) model. This new scheme is discussed in detail by Lawrence and Chase (2009). This experiment also uses land surface characteristics derived from MODIS continuous vegetation fields as described in Section 3.1.2 and also in topographic slope data. The

purpose of the CLM–SiB experiment is to address the low contributions from transpiration and high contributions from canopy and soil evaporation found with the release CLM 3.0. Lawrence and Chase (2009) found that implementation of SiB in CLM3 leads to substantial increases in transpiration (15–42%) and substantial decreases in canopy evaporation (38–24%) and soil evaporation (47–34%), respectively. The changes in the evapotranspiration partition make CLM–SiB consistent with the consensus of other land surface models used in Global Circulation Models, which have average global evapotranspiration dominated by transpiration (47%), with substantially smaller contributions from evaporation from canopy intercepted precipitation (17%) and bare soil (36%) (Dirmeyer *et al.*, 2005). The CCSM configuration for the CLM–SiB experiment also includes a different parameterisation for sea ice compared to the model configurations used for the CONTROL and CLM–MODIS experiments. In the configuration used for the CLM–SiB experiment, the Data Sea Ice Model component of CCSM has been replaced by the Community Sea Ice Model (CSIM), constrained with the spatial extent defined by an observed sea ice climatology for 1970–2001.

3.2. Satellite-derived climatology of TOA fluxes

The CERES instrument provides broadband radiometric measurements of the Earth's atmosphere for three

channels: shortwave (0.3–5.0 μm), total (0.3–200 μm), and longwave infrared (8–12 μm). We use the observations from the CERES FM1 instrument on board the Terra Earth Observation Satellite, which has an overpass time of approximately 10:30 am local time. In addition to numerous other data products, derived parameters in the ERBE-like ES-9 collection include monthly averages of planetary albedo and TOA shortwave and longwave fluxes for both all-sky and clear-sky conditions. The CERES measured radiances are converted to TOA fluxes using angular distribution models (ADMs) for specific scene types. These TOA SW fluxes are used to derive broadband albedos for cloud-free regions and upwelling longwave radiation at the TOA. CERES FM1 data are available beginning in March 2000 and continue to be processed to this day, providing a 7-year time series to analyse climatic trends in TOA shortwave and longwave radiation. We use primarily FM1 data as the FM1 instrument is generally in cross-track mode, providing the maximum spatial sampling compared to along track and RAP scanning strategies. Prior to January 2002, FM1 was occasionally operated in one of these other modes and for these months, for which data from the identical FM2 instrument operating in cross-track mode were substituted. The time period considered in this study is from March 2000 to May 2007. Further details are found in Loeb *et al.* (2005, 2007). The TOA SW fluxes have a small positive bias of 0.2 W m^{-2} for regional monthly averages and root mean square (RMS) errors between 0.7 and 1.4 W m^{-2} .

In ERBE-like processing, the instantaneous CERES measurements of radiances are first converted to fluxes using angular distribution (or directional) models. The instantaneous clear-sky fluxes are further diurnally averaged using diurnal models even though clear-sky conditions might have existed only for a small part of the day. The monthly averages are constructed using the ‘daily’ data that had been diurnally averaged. There are two common methods adopted in GCMs to compute ‘clear-sky’ fluxes (Cess *et al.*, 1992). In Method I, the clear-sky pixels are isolated over a time period and then averaged; whereas in Method II the clear-sky fluxes are computed in ‘clear-sky mode’ for all instances and then time averaged. Neither one of these methods is entirely analogous to ERBE-like processing. In Method I, the clear-sky values are isolated but this approach lacks the diurnal averaging employed by ERBE-like algorithm adopted by CERES E9. Method II incorporates diurnal averaging but may suffer from negative bias in transmissivity under cloudy conditions due to enhanced water vapour in the atmosphere. The CCSM3 approach is based on Method II that has been deemed to be more appropriate for intercomparisons (Cess *et al.*, 1992).

3.3. Quantifying systematic biases in CCSM3 simulation of $S_{\text{TOA}}^{\uparrow}$

Comparison between CCSM-simulated and CERES estimates of $S_{\text{TOA}}^{\uparrow}$ (discussed later in Section 4) suggested that there are systematic biases in the CCSM3 simulation

of $S_{\text{TOA}}^{\uparrow}$. This study quantifies the bias using statistical relationship between bulk atmospheric transmissivity in the shortwave, computed from observations to that simulated by radiative transfer parameterisation used by CCSM3. Data needed for this purpose, radiosonde profiles at relatively high temporal resolution and surface pyranometer observations, are available at two sites considered in this study: the SGP-CF of the ARM program in Oklahoma and its Mobile Facility in Niger, Africa. The following formulation is used for estimating the error introduced by systematic bias in the CCSM3 computation of $S_{\text{TOA}}^{\uparrow}$. Instantaneous value of upwelling shortwave flux at the TOA is given by:

$$F_{\text{TOA}}^{\uparrow}(t) = \alpha F_0 \mu(t) \tau^2(t) \quad (1)$$

In Equation (1), α , F_0 , μ and τ denote surface albedo, solar constant, cosine of SZA and bulk transmissivity of the atmospheric column. The bulk transmissivity is given by:

$$\tau = \frac{F_{\text{surf}}^{\downarrow}}{\mu F_0} \quad (2)$$

$F_{\text{surf}}^{\downarrow}$ is the CCSM-computed downwelling shortwave flux at the surface. The diurnally averaged upwelling shortwave flux at the TOA is given by:

$$\begin{aligned} S_{\text{TOA}}^{\uparrow} &= \frac{1}{L} \int_0^{24\text{hr}} F_{\text{TOA}}^{\uparrow}(t) dt \\ &= \frac{\alpha F_0}{L} \int_0^{24\text{hr}} \mu(t) \tau^2(t) dt = \alpha F_0 \xi \end{aligned} \quad (3)$$

where L is 24 h and ξ is given by the following equation:

$$\xi = \frac{1}{L} \int_0^{24\text{h}} \mu(t) \tau^2(t) dt \quad (4)$$

If the actual value of bulk transmissivity for the atmospheric column is τ_0 , then the error introduced by the biased estimate of τ is given by:

$$\Delta_{\text{TOA}}^{\uparrow}(t) = \alpha F_0 \mu(t) \tau_0^2(t) - \alpha F_0 \mu(t) \tau^2(t) \quad (5)$$

where τ_0 is given by the following equation:

$$\tau_0 = \frac{F_{\text{surf,obs}}^{\downarrow}}{\mu F_0} \quad (6)$$

$F_{\text{surf,obs}}^{\downarrow}$ in Equation (6) denotes the observed downwelling shortwave flux received at the surface. The diurnally averaged error estimate is given by:

$$\begin{aligned} \overline{\Delta_{\text{TOA}}^{\uparrow}}(t) &= \alpha F_0 \frac{1}{L} \int_0^{24\text{hr}} \mu(t) \tau_0^2(t) dt \\ &\quad - \alpha F_0 \frac{1}{L} \int_0^{24\text{hr}} \mu(t) \tau^2(t) dt \\ &= \alpha F_0 \xi_0 - \alpha F_0 \xi \end{aligned} \quad (7)$$

ξ_0 is defined in Equation (8).

$$\xi_0 = \frac{1}{L} \int_0^{24h} \mu(t) \tau_0^2(t) dt \quad (8)$$

Equation (5) can be further simplified as:

$$\overline{\Delta}_{TOA}^\uparrow(t) = \alpha F_0 \xi \left[\frac{\xi_0}{\xi} - 1 \right] = S_{TOA}^\uparrow \left[\frac{\xi_0}{\xi} - 1 \right] \quad (9)$$

Bias in CCSM3 computed atmospheric transmissivity is quantified by an empirical function fit between ξ and ξ_0 . Radiosonde and pyranometer observations from the ARM sites in Oklahoma and Niger for all available clear days in 2007 and 2006, respectively, are utilised for this purpose. Observations of downwelling shortwave flux at the surface ($F_{surf,obs}^\downarrow$) from the pyranometer, available at 1-min intervals, are used along with Equations (6) and (8) to compute ξ_0 at 15-min intervals. The Column Radiation Model (CRM), a stand-alone version of the radiative transfer scheme used in CCSM3, is used to compute F_{surf}^\downarrow which is used along with Equations (2) and (4) to calculate ξ . Note that in the CRM computations, linear interpolation of radiosonde observations available at 6-h intervals, is used to specify a time-varying atmospheric thermodynamic profile. The column ozone profile, assumed to be diurnally invariant, is specified using profiles obtained from the European Centre for Medium-Range Weather Forecasts (ECMWF) 45-year reanalysis (ERA-40) dataset. Observed aerosol optical depth (AOD) is utilised in the CRM computations for the Niger site, while a constant background value is assumed for the Oklahoma site where the AOD information is not available. Linear regression between ξ and ξ_0 yields (Figure 2(a) and (b)) a statistical prediction equation for ξ .

The procedure for estimating errors associated with systematic biases in CCSM3 computation of S_{TOA}^\uparrow is as follows. For a particular CCSM grid point, a monthly averaged climatological atmospheric moisture profile from the ERA is first scaled by the CCSM monthly averaged integrated precipitable water vapour (PWV) values. Then this scaled atmospheric moisture profile is used in CRM to compute ξ assuming diurnal variation of SZA consistent with mid-month of day conditions. The computed value of ξ is then used along with the statistical prediction equation obtained from linear regression (Figure 2(a) and (b)) to compute the expected value of ξ_0 , which is then used in Equation (9) along with the CRM-computed value of ξ and the CCSM3-computed S_{TOA}^\uparrow value to yield the error estimate.

Note that ξ_0 and ξ are proportional to observational and CCSM-computed estimates of bulk atmospheric transmissivity. At the Niger site, CCSM computation of atmospheric transmissivity is an overestimate compared to observational estimates (Figure 2(a)). However, over the ARM Central Facility site in Oklahoma, the CCSM estimate of bulk transmissivity is clearly an overestimate only for ξ values in excess of 0.15 (Figure 2(b)). This

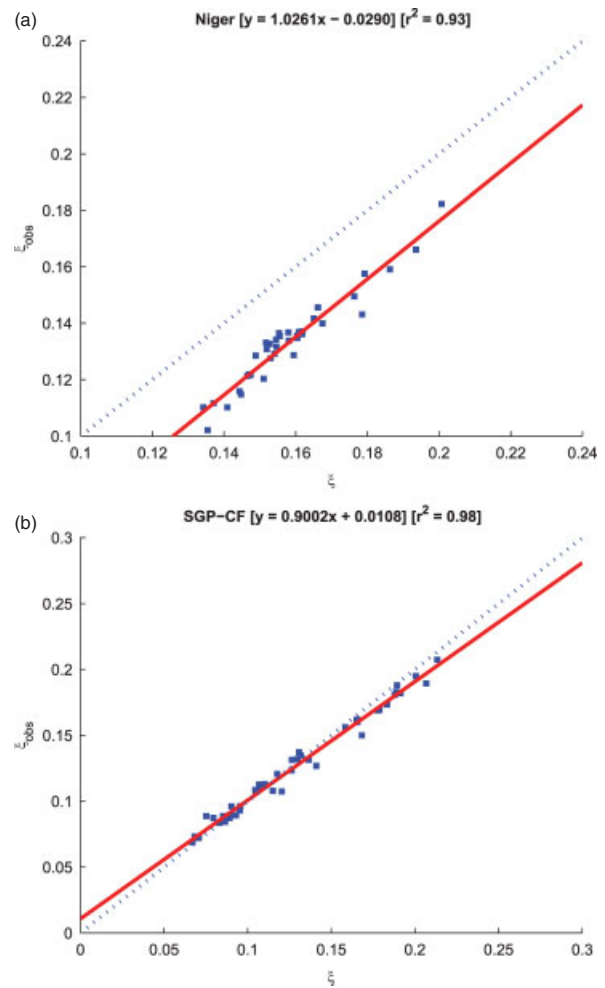


Figure 2. Scatterplot between ξ and ξ_0 , parameters that are correlated to CCSM-computed and observational estimates of bulk atmospheric transmissivity for: (a) the ARM Niger site in Africa, and (b) the ARM central facility site in Oklahoma. The solid line is the linear regression fit and the dashed line is a one-to-one curve. The equation describing the linear fit is given within each panel and the RMS errors are 0.787 and 0.9848 for the Niger and Oklahoma sites, respectively. This figure is available in colour online at wileyonlinelibrary.com/journal/joc

error analysis suggests that the CCSM radiative transfer parameterisation tends to overestimate atmospheric transmissivity and that the magnitude of the error shows geographic variation.

4. Results

The CCSM3-simulated clear-sky S_{TOA}^\uparrow from the CONTROL, CLM-MODIS and CLM-SiB simulations is compared against corresponding CERES observations. Monthly averaged S_{TOA}^\uparrow from the last 10 years of these experiments are computed and then the averages for the months of DJF, MAM, JJA and SON (corresponding to NH winter, spring, summer and autumn seasons) are computed. The monthly averaged CERES S_{TOA}^\uparrow data are resampled to the CCSM domain and then the averages for seasonal categories are computed.

Comparison between the CERES-observed S_{TOA}^\uparrow and the corresponding values in model simulations show

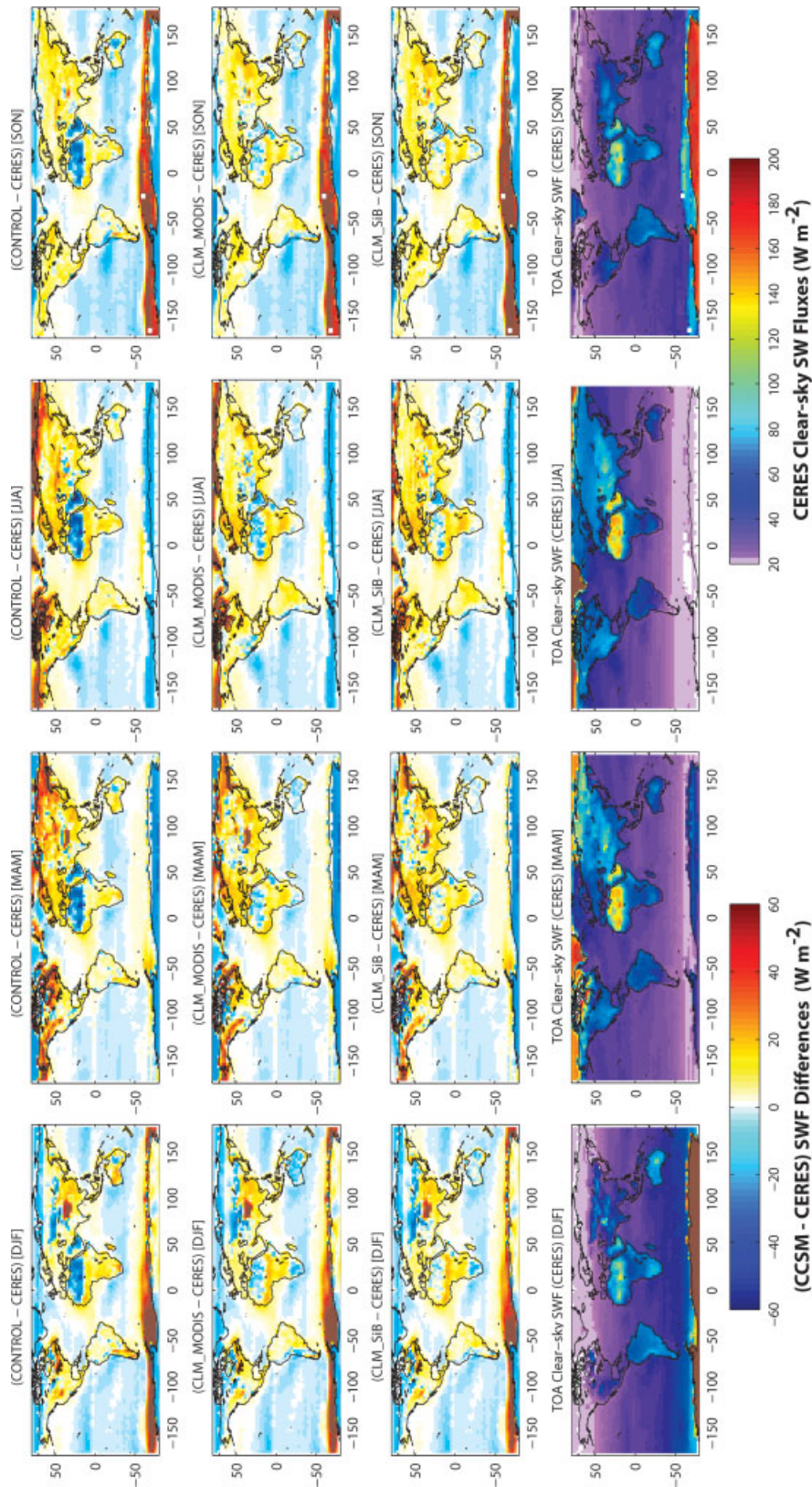


Figure 3. Seasonal variation of CERES observations and the differences in global averages of TOA upwelling SW flux between CCSM and CERES for current land use CONTROL, CLM-MODIS, CLM-SiB and potential vegetation. This figure is available in colour online at wileyonlinelibrary.com/journal/joc

substantial differences (Figure 3). On average, CCSM simulation experiments overestimate S_{TOA}^{\uparrow} compared to CERES observations over both land and ocean by approximately 1.6 W m^{-2} and 7.6 W m^{-2} , respectively. However, substantial regional variations exist over both land and ocean, with the experiments overestimating S_{TOA}^{\uparrow} over some regions (e.g. Tibetan Plateau, Arctic Ocean) and underestimating it over others (e.g. Saharan Desert, Southern Equatorial Ocean areas).

4.1. Regional differences

4.1.1. Polar oceans

Compared to CERES observations, significant positive biases in S_{TOA}^{\uparrow} (in excess of 40 W m^{-2}) are observed over the Arctic Ocean region in both the CONTROL and CLM–MODIS experiments during the boreal summer months (Figure 3). The positive bias in S_{TOA}^{\uparrow} over the Arctic Ocean is substantially reduced in the CLM–SiB experiment which incorporates an improved representation of sea ice. Over the Southern Ocean, during the austral summer months of DJF, the CONTROL, CLM–MODIS and CLM–SiB experiments all show a belt of strong positive bias (in excess of 40 W m^{-2}) extending from the coast of the Antarctic continent into the Southern Ocean. This feature is also present during the austral spring months of SON, but with reduced northward extent into the Southern Ocean. In the Southern Ocean region, the impact of improved sea ice parameterisation appears to be less effective compared to the Arctic Ocean area.

4.1.2. High latitude land areas and mountain regions

In comparison to CERES observations, all three CCSM experiments show seasonally varying regions of strong positive bias in S_{TOA}^{\uparrow} along the land areas north of 60°N latitude (Figure 3). These regions include Alaska, regions of North America east of the Great Lakes, northern coasts of Eurasia and the eastern Pacific seaboard of Russia. The positive biases that occur during the boreal spring and summer months over high latitude regions in the NH are more prominent during the months of MAM and persist over the eastern regions of North America during the months of JJA but are then non-existent during the other months. The differences between CERES and the model simulations are most pronounced for the CONTROL, least for the CLM–SiB and moderate for the CLM–MODIS experiment. Note that over land areas, the effect of snow cover on albedo is very different depending upon the nature of land use. The improved performance of CLM–MODIS and CLM–SiB simulations is potentially related to improvements in: (1) simulated precipitation fields due to more realistic specification of land surface characteristics; and (2) values of computed composite albedo in regions of snow cover, which is parameterised as a function of snow and land surface albedo.

During the boreal spring and summer months, all three experiments show substantial positive biases in S_{TOA}^{\uparrow}

over the Tibetan Plateau when compared to CERES observations (Figure 3). Annual variation of average S_{TOA}^{\uparrow} patterns from CERES observations and the three CCSM simulations (Figure 4(a) and (b)) shows that the patterns from the experiments are radically different compared to CERES observations. Over the Tibetan Plateau region, all three experiments show the S_{TOA}^{\uparrow} values in excess of 250 W m^{-2} during the month of May whereas CERES observations show an average value of $\sim 103 \text{ W m}^{-2}$ (Figure 4(a)). Correspondingly, surface albedo from all three experiments shows an anomalous trend (Figure 4(b)) whereas the MODIS visible albedo shows only a slight deviation. The closest agreement between the experiments and observations is found during the time period of July to September after which the differences become substantial.

One of the possible reasons for the substantial differences observed over high latitude sites is the inability of coarse resolution GCM simulation experiments to resolve

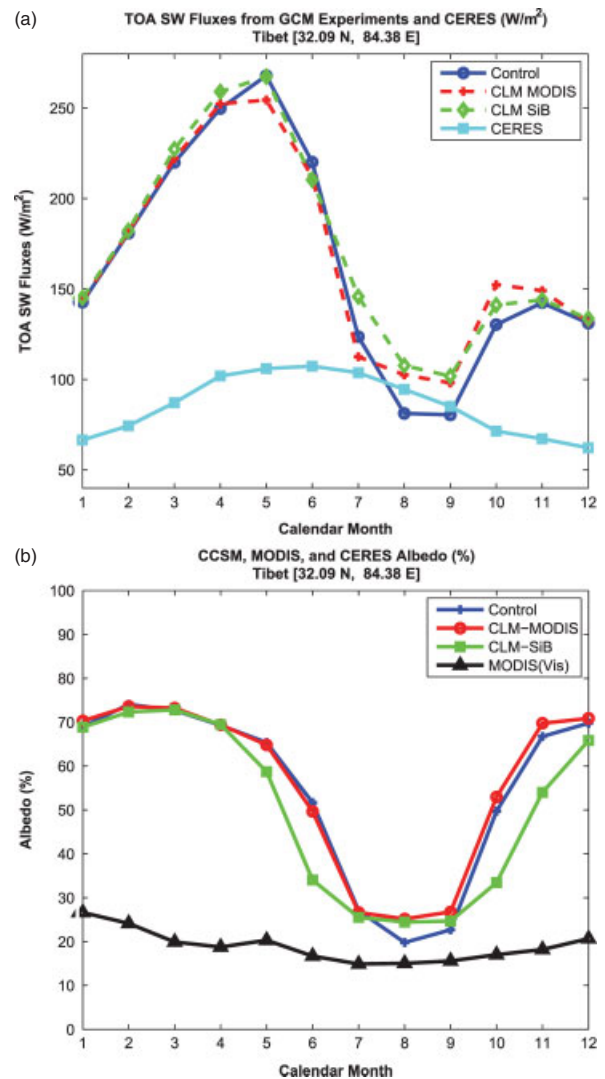


Figure 4. Seasonal variation of the model-simulated and CERES-observed S_{TOA}^{\uparrow} (top), and model-computed and MODIS-derived albedo (bottom) over the Tibetan Plateau. This figure is available in colour online at wileyonlinelibrary.com/journal/joc

the spatial variability of snow cover. Orographic forcing causes a significant amount of snowfall to occur at higher altitudes where the snow cover persists on the ground and/or vegetation canopies due to colder temperatures and/or lower radiative heating. Coarse resolution GCMs are unable to resolve this spatial heterogeneity of snow cover, snow depth, snow age and snow melt (Flanner and Zender, 2005; Dickinson *et al.*, 2006; Qu and Hall, 2006; Roesch, 2006) and distribute the snow cover uniformly within the grid cell resulting in overestimation of the surface albedo. Dickinson *et al.* (2006) also note that the observed lower albedos would lead to increased warming with further melting of snow and a decrease in snow cover.

Note that CERES clear-sky observations over the high altitude sites used to estimate S_{TOA}^{\uparrow} may also be biased due to the deficiencies in cloud masking algorithms that traditionally fare poorly over regions of snow and ice cover. However, the impact of these deficiencies on CERES S_{TOA}^{\uparrow} estimates is not clear.

4.1.3. Deserts

Compared to CERES observations, the CONTROL experiment underestimates S_{TOA}^{\uparrow} over some of the major deserts around the globe including the Sahara, Arabian, Gobi, Atacama and eastern part of the Great Australian Desert (Figure 3). Over the Mojave, Sonoran, Namib, Kalahari and western parts of the Great Australian Desert, the CONTROL experiment overestimates S_{TOA}^{\uparrow} . In general, the experiments constrained by MODIS observations improve simulated seasonal variation of S_{TOA}^{\uparrow} with CLM–SiB showing the best agreement compared to CERES observations.

The differences in S_{TOA}^{\uparrow} between the CONTROL experiment and CERES observations are most striking for the Saharan and Arabian Deserts. Annual variations of monthly mean S_{TOA}^{\uparrow} over the Chad region in the Saharan Desert show the CONTROL experiment significantly underestimating S_{TOA}^{\uparrow} compared to CERES observations with the differences consistently exceeding 15 W m^{-2} throughout the year. Maximum differences in excess of 30 W m^{-2} are found during the JJA months (Figure 5(a)). Both experiments utilising MODIS to constrain land surface albedo show significant improvement in simulated S_{TOA}^{\uparrow} . Both the experiments underestimate S_{TOA}^{\uparrow} compared to CERES, but the magnitude of differences rarely exceed 5 W m^{-2} . The CLM–SiB experiment shows better performance compared to CLM–MODIS, but the difference in S_{TOA}^{\uparrow} between the two experiments rarely exceeds 1 W m^{-2} (month of August) with the CLM–SiB experiment showing consistently higher values.

Analysis conducted in Section 3.3 shows that there is a systematic bias in CCSM computation of bulk atmospheric transmissivity. To understand the implications of the systematic model biases in comparison between simulated and observed values of S_{TOA}^{\uparrow} , the annual cycles of S_{TOA}^{\uparrow} over the ARM site in Niger is considered

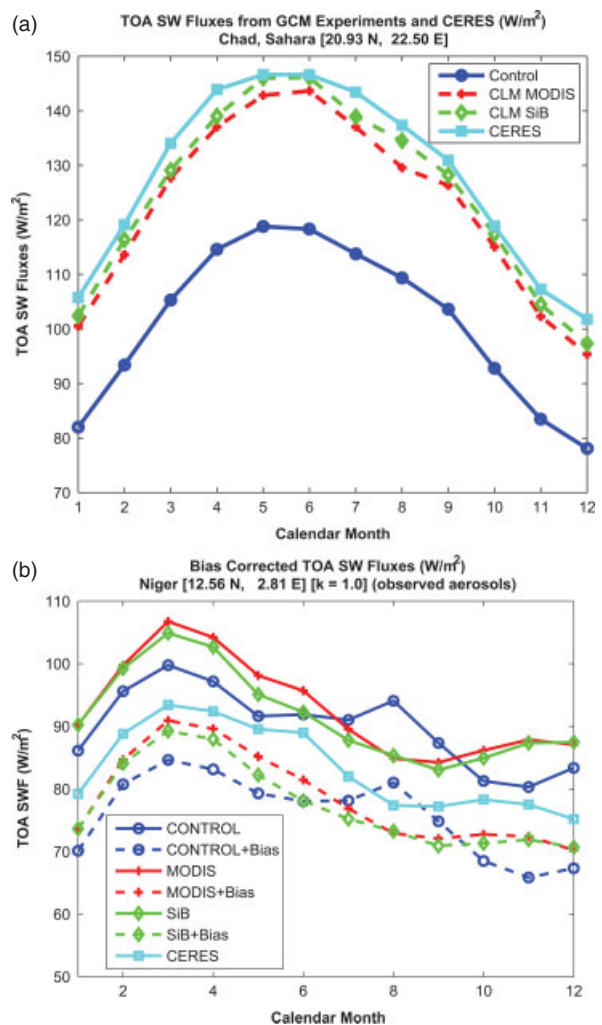


Figure 5. Seasonal variation of CERES-observed and CCSM-simulated S_{TOA}^{\uparrow} over Chad, Sahara (top) and ARM Mobile Facility at Niamey, Niger (bottom). The dashed lines in (b) indicate the bias-corrected values for the respective CCSM experiments. This figure is available in colour online at wileyonlinelibrary.com/journal/joc

(Figure 5(b)). At the Niger location, both the CONTROL and CLM–MODIS experiments overestimate S_{TOA}^{\uparrow} compared to CERES observations, with the estimates from the CONTROL experiment being closer to CERES observations. Thus it would appear that use of MODIS data to constrain the land surface albedo produces the opposite result compared to the Chad site, making the GCM simulation of S_{TOA}^{\uparrow} worse. However, application of the procedure described in Section 3.3 to account for systematic biases in both the radiative transfer parameterisation and column water vapour loading shows that improvements in simulation of S_{TOA}^{\uparrow} through the use of MODIS data are masked by systematic biases in the GCM. Once the bias corrections are applied (Figure 5(b)), both CLM–MODIS and CLM–SiB are in better agreement with CERES than the CONTROL simulation. Though the CONTROL apparently seems to match CERES during the rainy period in August, the prevailing trend is opposite to that of CERES in the preceding and following months. Hence, the prescription of land surface parameters based

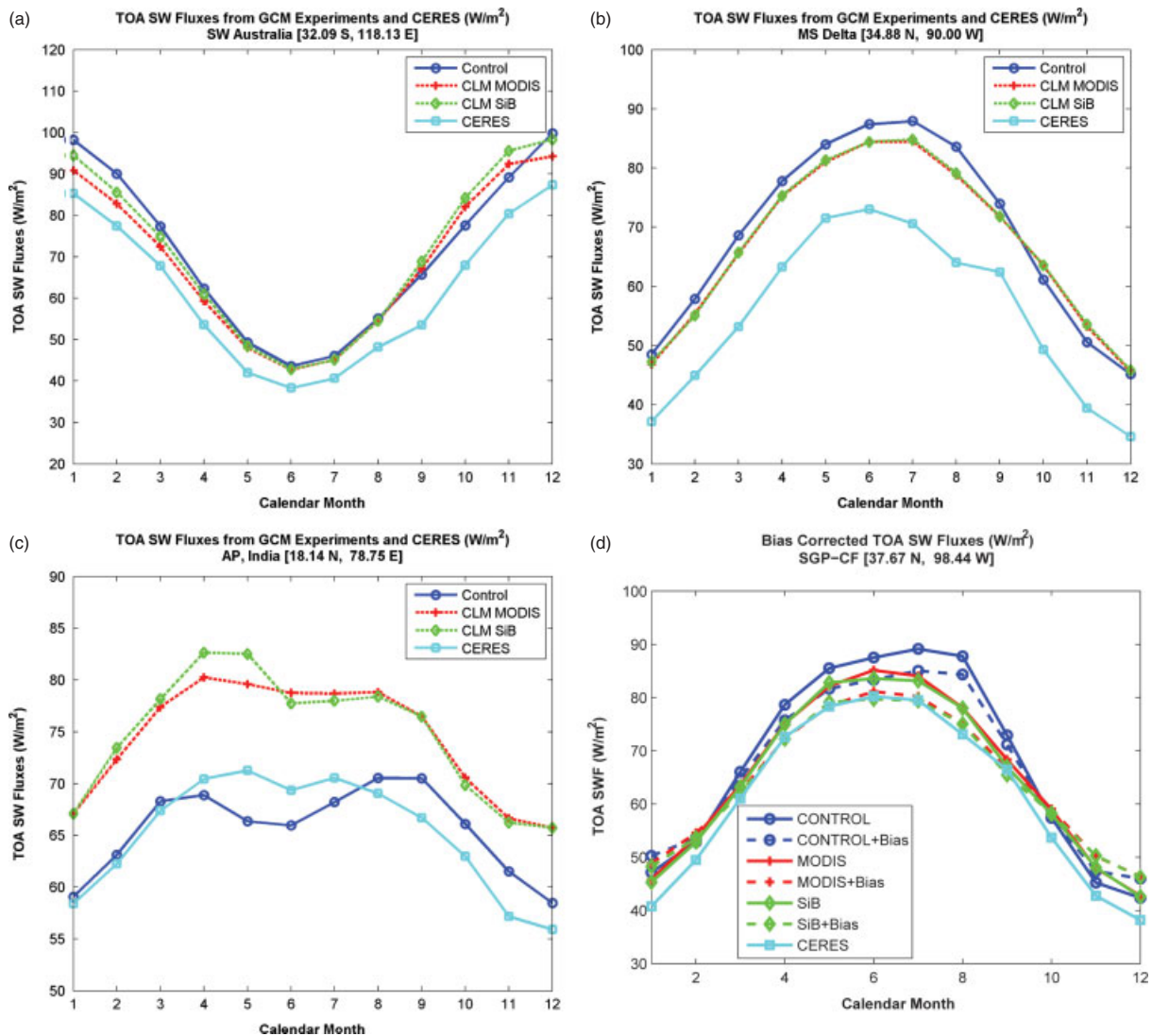


Figure 6. Clear-sky TOA SW fluxes (monthly averaged) over agricultural and mixed cropland regions over the (a) SW Australia; (b) Mississippi Delta; (c) central Andhra Pradesh in India; and (d) SGP Central Facility in Lamont, OK. The dashed lines in (d) indicate the bias-corrected values for the respective CCSM experiments. This figure is available in colour online at wileyonlinelibrary.com/journal/joc

on MODIS has resulted in overall improvement after the bias corrections, with CLM–MODIS exhibiting the best agreement.

4.1.4. Agricultural regions

Nair *et al.* (2007) suggested that use of satellite-derived land surface characteristics has the potential to improve $S_{\text{TOA}}^{\uparrow}$ over agricultural areas since such data better capture phenological changes associated with anthropogenic agricultural activities. However, comparison of $S_{\text{TOA}}^{\uparrow}$ from CONTROL, CLM–MODIS and CLM–SiB over selected sites of agricultural land use shows mixed response to the use of MODIS-derived land surface characteristics to constrain the GCM.

All three experiments consistently overestimate $S_{\text{TOA}}^{\uparrow}$ over southwest Australia, where 13 million hectares of native vegetation was cleared for agriculture (Figure 6(a)). During the fallow period (December, January

to March), CLM–MODIS-simulated $S_{\text{TOA}}^{\uparrow}$ shows closest agreement to CERES observations followed by the CLM–SiB experiment. However, during the months of October and November, $S_{\text{TOA}}^{\uparrow}$ in the CONTROL experiment shows closest agreement to CERES observations. Over the Mississippi Delta region in the southern United States, $S_{\text{TOA}}^{\uparrow}$ is consistently overestimated by all three experiments (Figure 6(b)). The CLM–MODIS and CLM–SiB experiments show closest agreement to CERES observations, except during the months of October and November during which the CONTROL experiment exhibits better performance. The CONTROL experiment shows superior performance over Hyderabad, India (Figure 6(c)), with the simulated $S_{\text{TOA}}^{\uparrow}$ agreeing very well with CERES observations during the first 4 months of the year. The CLM–MODIS and CLM–SiB experiments significantly overestimate $S_{\text{TOA}}^{\uparrow}$ compared to both the CONTROL experiment and CERES observations. Both the CLM–MODIS and CLM–SiB-simulated

$S_{\text{TOA}}^{\uparrow}$ are very similar except during the months of April and May during which the CLM–SiB-simulated values are slightly higher. Yet different behaviour is observed over the ARM Central Facility Site in Oklahoma (Figure 6(d)). All the experiments overestimate $S_{\text{TOA}}^{\uparrow}$, but CLM–MODIS and CLM–SiB-simulated $S_{\text{TOA}}^{\uparrow}$ show closest agreement to CERES observations during the time period of March to September while there is better agreement between the CONTROL experiment and observations during the rest of the time period. Note that the CLM–MODIS and CLM–SiB simulations of $S_{\text{TOA}}^{\uparrow}$ most deviate from CERES observations during the winter months when a substantial amount of precipitation is in the form of snow.

Differing responses to the use of MODIS-derived land surface characteristics to constrain GCM simulation experiments is due to differences in simulated surface precipitation fields and systematic biases in CCSM radiative transfer computation, both of which exhibit geographic variation. Feedbacks associated with changes in land surface characteristics alter evapotranspiration and precipitation which contributes to differences in $S_{\text{TOA}}^{\uparrow}$ between the CLM–MODIS and CLM–SiB experiments.

The impact of systematic biases in radiative transfer computation, using the methodology outlined in Section 3.3, is examined for one agricultural site, the ARM Central Facility in Oklahoma. This analysis improves the agreement between CERES observations and simulated values of $S_{\text{TOA}}^{\uparrow}$ from all the experiments. However, the best agreement is found between CLM–MODIS, CLM–SiB and the CERES observations. If this trend in systematic bias found for the ARM site is also applicable to the other agricultural sites, qualitatively accounting for the systematic biases, the use of MODIS data in the CLM–MODIS and CLM–SiB experiments improves the agreement between GCM-simulated $S_{\text{TOA}}^{\uparrow}$ and observations for the sites in the Mississippi Delta, Western Australia and India. At the Indian site (Figure 6(c)), the bias correction procedure could potentially alter the simulated $S_{\text{TOA}}^{\uparrow}$ from the CONTROL experiment to be an underestimate and that from the CLM–MODIS and CLM–SiB experiments to be in closer agreement to CERES observations.

4.1.5. Forested regions

All three experiments generally overestimate $S_{\text{TOA}}^{\uparrow}$ when compared to CERES observations in forested regions. In contrast to agricultural sites, the differences between the CONTROL, CLM–MODIS and CLM–SiB simulations are substantially smaller for the forested sites with the exception of Borneo (Figure 7(a)–(d)). The pattern of annual variation of $S_{\text{TOA}}^{\uparrow}$ in the CLM–MODIS and CLM–SiB experiments is in better agreement with CERES observations for most of the forest sites. For the Amazon sites, the $S_{\text{TOA}}^{\uparrow}$ in the CONTROL experiment agrees closely with CLM–MODIS and CLM–SiB except during the latter part of the wet season (JJA for the northern site and DJF for the southern site) and the

beginning part of the dry season. Over the Congo site, the CLM–MODIS and CLM–SiB simulations are in close agreement throughout the year, while the CONTROL experiment deviates from these experiments during the time period of March to December, though never in excess of 3 W m^{-2} . Over the Borneo site, CLM–MODIS and CLM–SiB are in agreement with each other, but the patterns of annual variation differ compared to observations. For example, the CERES observations show a decreasing trend in $S_{\text{TOA}}^{\uparrow}$ during the November to December time period, while the CLM–MODIS and CLM–SiB experiments show the simulated values being steady during the same period. The CONTROL experiment shows a decreasing trend in agreement to observed patterns during this time period, but differs during the March to August time period.

4.1.6. Tropical and mid-latitude oceans

Over tropical and mid-latitude ocean areas, CCSM experiments generally underestimate $S_{\text{TOA}}^{\uparrow}$ ($\sim 5 \text{ W m}^{-2}$) over most of the Southern Hemisphere. However, in the NH, significant areas over which $S_{\text{TOA}}^{\uparrow}$ is overestimated exist in the North Atlantic Ocean, Arabian Sea, Bay of Bengal, Indian Ocean and the northern Pacific Ocean (Figure 3). Differences in $S_{\text{TOA}}^{\uparrow}$ between CERES and CCSM experiments show substantial spatial variability across the seasons in the NH with the regions where $S_{\text{TOA}}^{\uparrow}$ is overestimated expanding to include significant portions of the Atlantic and Indian Ocean in the boreal summer months of JJA. In the Southern Hemisphere, bias patterns show less seasonal variability but the magnitude of underestimation varies with season and the minimum differences found during the months of MAM. The zonal averages of the differences between CCSM simulations and CERES are more or less comparable across the latitudes except for the polar regions where the CLM–SiB simulations are distinctly different from the CONTROL and CLM–MODIS experiments (Figure 8).

5. Discussion

Findings from the error analysis conducted over the two ARM observational sites (see Section 3.3) where CCSM3 underestimates atmospheric attenuation of solar radiation is consistent with prior studies that suggest that broadband radiative transfer models often overestimate total irradiance reaching the surface. Under clear-sky conditions, errors of up to $40\text{--}50 \text{ W m}^{-2}$ (10%) may occur at high solar angles (Kato *et al.*, 1997; Kinne *et al.*, 1998; Tarasova *et al.*, 1999; Tarasova and Fomin, 2000), with a substantial portion of the errors resulting from improperly accounting for the effects of the water vapour continuum. Recently, Wild *et al.* (2008) analysed the radiation budget of 14 GCMs used in the IPCC-AR4 and CMIP3 simulations. The majority of the models tend to be excessively transparent to the shortwave radiation under both cloudy and clear-sky conditions. This anomalous surface insolation is attributed to the underestimation of water

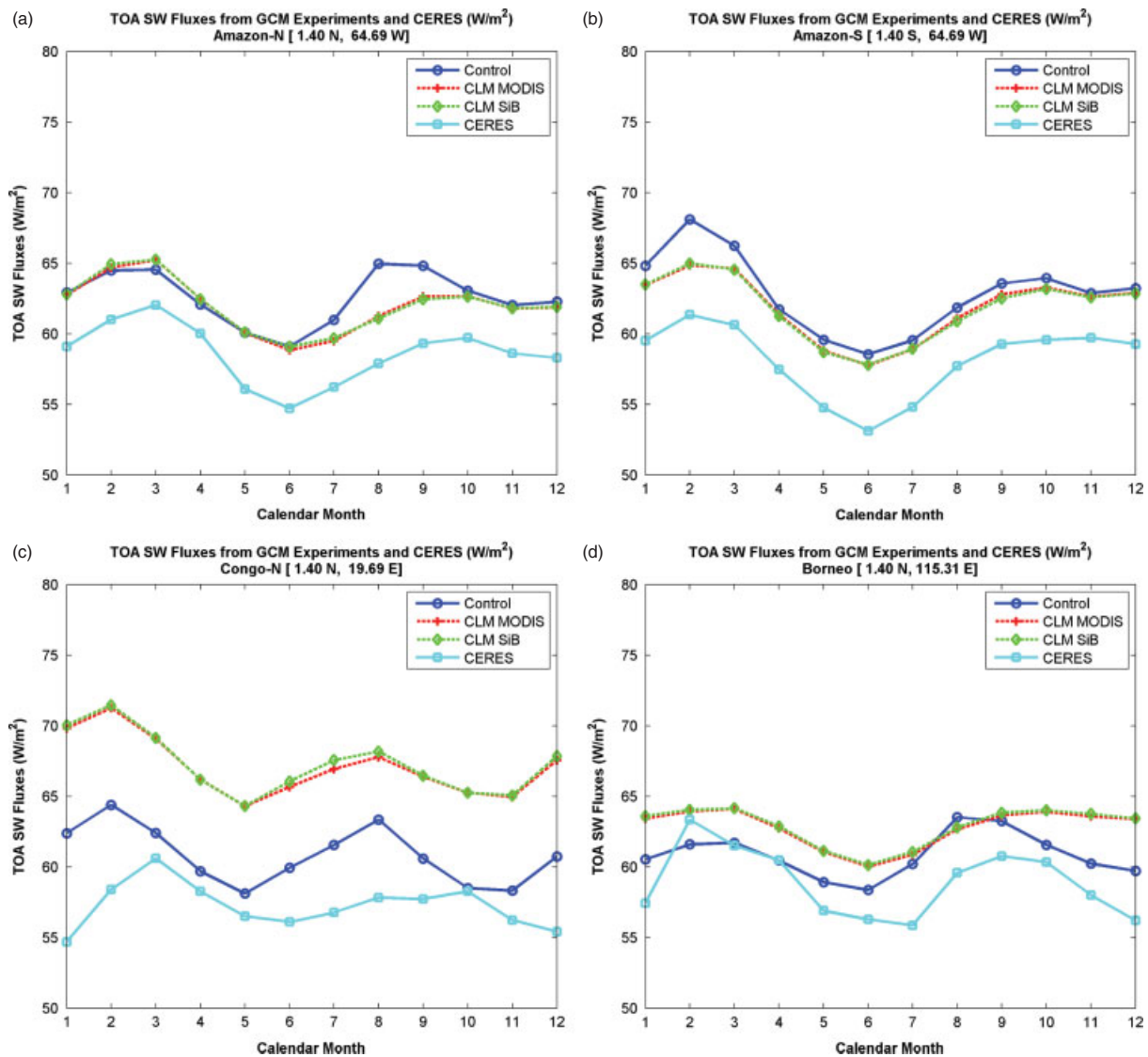


Figure 7. Clear-sky TOA SW fluxes over tropical forests over (a,b) Amazon; (c) Congo; and (d) Borneo. This figure is available in colour online at wileyonlinelibrary.com/journal/joc

vapour absorption in the GCM radiation codes. Models with improved spectroscopic data had more realistic shortwave absorption. On average, the models overestimated the downward shortwave radiation by 6 W m^{-2} which is an improvement from 10 W m^{-2} estimated by the models a decade ago (Wild, 1995). It was also noted by Wild *et al.* (2008) that the NCAR CCSM did have the best overall agreement among AR4 and CMIP3 models with the surface observations with a mean global bias of $+0.8 \text{ W m}^{-2}$. However, our results from the two different sites indicate that the regional biases may be substantially higher.

We also examined the impact of aerosol uncertainties on bias computations for the Niamey site. These aerosol sensitivity experiments show that our methodology is only marginally responsive ($<1 \text{ W m}^{-2}$ when annually averaged) to aerosol uncertainties at this location. Furthermore, over desert regions, Patadia *et al.* (2009) noted that the effect of dust on upwelling shortwave TOA is not substantial.

In the bias estimation methodology, we have assumed that the atmospheric transmission is nearly the same for both incoming and reflected solar radiation (Equation (8)); however, the bulk transmissivity for reflected radiation is often less than that of incoming solar radiation due to the spectral distribution of intensities of the reflected radiation. We examined the impact of reduced bulk transmissivity to reflected radiation by replacing the exponent of τ in Equation (8) with $1 + k$. The bias computations for the Niamey and SGP sites were repeated by varying the value of k from 1 to 0. When $k = 1$, the transmissivity is the same for both incoming and reflected radiation and when $k = 0$ the transmissivity for reflected radiation is unity. A value of k between 1 and 0 thus corresponds to variations in transmissivity for reflected radiation ranging for the same value as transmissivity of incoming radiation to a completely transparent atmosphere. Sensitivity studies show that, while better agreement between the CRM-simulated values and CERES observations is obtained for values of $k \sim 0.3$,

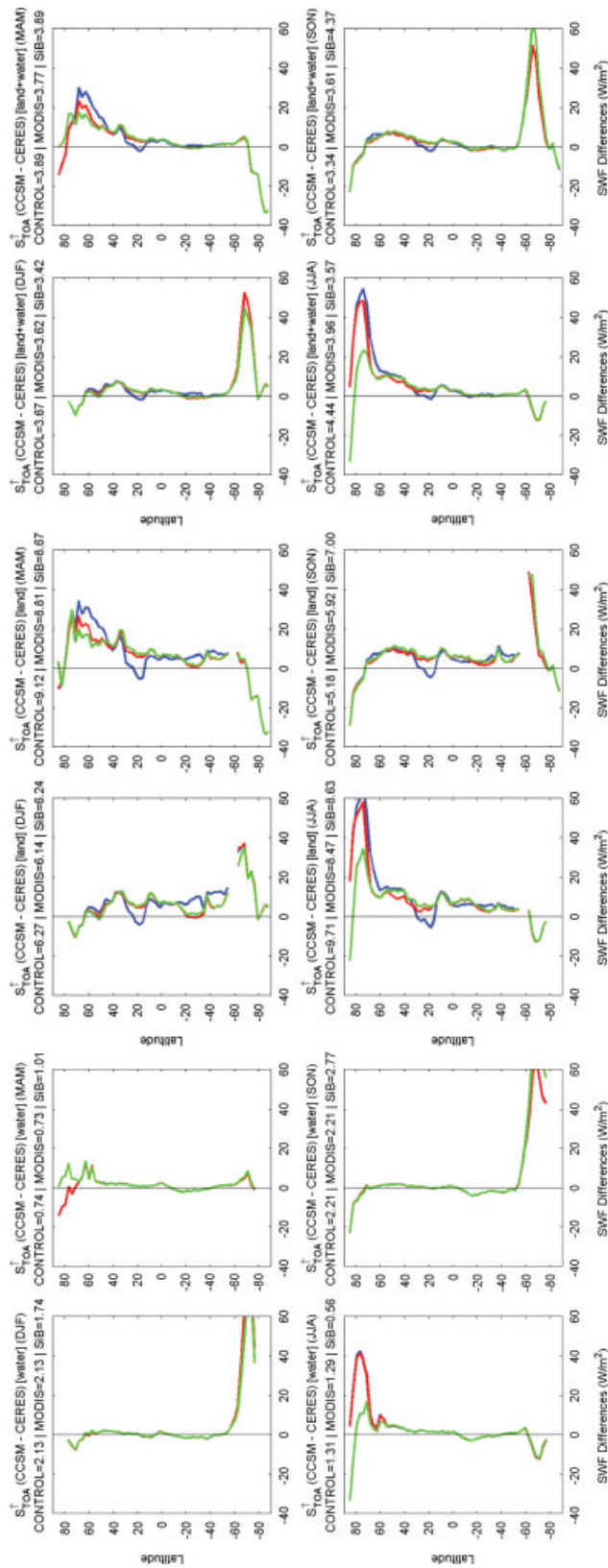


Figure 8. Zonal area-weighted averages of the differences in S_{TOA}^{\uparrow} between CCSM simulations (CONTROL – Blue; CLM-MODIS – Red; and CCSM – Green) and CERES; for water grid cells only (left); for land grid cells only (middle); and all (water + land) the CCSM grid cells (right). This figure is available in colour online at wileyonlinelibrary.com/journal/joc

bias correction is required for both Niamey and SGP sites. Hence, the interpretation of our results generally holds true for both the SGP and Niamey sites even when the assumption of equal transmissivity for incoming and reflected radiation is relaxed.

Underestimation of $S_{\text{TOA}}^{\uparrow}$ over desert regions by the standard version of CCSM3 reported in this study is also supported by prior studies. Oleson *et al.* (2003) compared surface albedo from the CLM to MODIS-derived land surface albedo and found that CLM underestimates albedo in the Saharan and Arabian Desert regions. Bender *et al.* (2006) examined the correlation between CERES observations of upwelling shortwave at the TOA for all-sky conditions and corresponding estimates from 20 GCMs used in IPCC assessments and found that the models in general poorly represent albedo variations over desert regions.

Globally, the impact of utilising MODIS-derived land surface albedo on CCSM simulations of $S_{\text{TOA}}^{\uparrow}$ appears minimal. Even over land areas, the maximum difference on an annual average basis is less than 0.23 W m^{-2} . However, seasonal differences are much more substantial with globally averaged $S_{\text{TOA}}^{\uparrow}$ over land areas for CLM–MODIS and CLM–SiB differing from the CONTROL experiment by 1.2 and 1.4 W m^{-2} , with the CLM–MODIS experiment showing closer agreement to CERES observations. Zonal-average difference plots show that CLM–SiB better simulates northern high latitude distribution ($45\text{--}80^{\circ}\text{N}$) of $S_{\text{TOA}}^{\uparrow}$ during MAM and in JJA (Figure 8).

Note that in the majority of the forest sites considered in this study, the impact of utilising MODIS observations on the simulation of $S_{\text{TOA}}^{\uparrow}$ is less compared to that for agricultural sites. This is consistent with the findings of Nair *et al.* (2007), suggesting that use of satellite-observed land surface characteristics have the potential to preferentially improve representation of the surface energy budget in GCMs over regions dominated by anthropogenic land use. Over forested sites, phenological patterns are more predictable and therefore easier to specify in a GCM, whereas over agricultural sites, use of satellite observations provides a distinct advantage of being able to capture complex phenological patterns that are difficult to parameterise.

Ocean Surface Albedo (OSA) is sensitive to SZA, wind speed and ocean chlorophyll concentration and is modulated by atmospheric aerosols and clouds (Jin *et al.*, 2004). The effect of wind speed on OSA can be substantial. Li *et al.* (2006) found differences of up to $10\text{--}20 \text{ W m}^{-2}$ in reflected solar flux at the TOA computed by radiative transfer models when only the SZA dependency of OSA is specified instead of both wind speed and SZA dependency. Wind speed dependency of OSA increases as the SZA increases. At SZAs of 80° , OSA almost doubles when wind speed changes from calm conditions to 15 m s^{-1} (Li *et al.*, 2006). The OSA parameterisations used in CCSM3 do not account for the effect of wind speed and may be responsible for bias patterns found in the CCSM3-simulated $S_{\text{TOA}}^{\uparrow}$ field. The seasonal

variation in bias patterns of $S_{\text{TOA}}^{\uparrow}$ is correlated to surface wind patterns (not shown). For example, note that the magnitude of CCSM-simulated $S_{\text{TOA}}^{\uparrow}$ over the Arabian Sea and Bay of Bengal is maximised during the boreal summer months when the surface wind speeds in this region are at a maximum. The CCSM OSA parameterisation does not consider wind speed effects and thus the CCSM overestimates OSA in this region causing the maximum positive bias in model computation of $S_{\text{TOA}}^{\uparrow}$.

However, other factors also need to be considered in addition to the wind speed effect, including systematic biases in radiative transfer computation that vary geographically (see Section 3.3) and also ocean colour which is impacted by chlorophyll concentration. Surface winds play a role in transporting nutrients from coastal areas and deeper waters modulating the growth of phytoplankton and thus ocean colour. The OSA parameterisations used in CCSM3 also do not account for ocean colour and its seasonal variation.

Over selected sites, simulation of annual variations in $S_{\text{TOA}}^{\uparrow}$ is improved through the use of MODIS-derived albedo to constrain CCSM3. Spatial patterns of seasonal-averaged $S_{\text{TOA}}^{\uparrow}$ also indicate the same (Figure 3), but seasonal averages tend to smooth features. In order to further validate this finding, correlation between monthly averaged values of $S_{\text{TOA}}^{\uparrow}$ from CERES observations and the three experiments are computed. Similar to Bender *et al.* (2006), geographical distribution of the correlation coefficients is examined (Figure 9(a)–(c)) and in all the experiments the CERES observations are found to be least correlated to simulated values in the region bounded by $10^{\circ}\text{N}\text{--}10^{\circ}\text{S}$. While the majority of other regions show high correlation, areas with smaller correlations are found over the Tibetan Plateau, land areas north of $\sim 40^{\circ}\text{N}$ and also along the periphery of the Antarctic continent. Note that the correlations progressively improve over North America, Russia, northern China and the northern part of South America in the CLM–MODIS and CLM–SiB experiments. Over central Africa, correlation improves in some areas while it becomes worse in other areas. Near the Antarctic, there is very little difference between CONTROL and CLM–MODIS while there is an improvement in CLM–SiB over this region. This analysis shows that the pattern of annual variation of $S_{\text{TOA}}^{\uparrow}$ is improved through the use of MODIS-derived albedo and the addition of the SiB land surface parameterisation further improves the performance of CCSM.

6. Conclusions

This study examines and compares the climatology of CCSM3-simulated $S_{\text{TOA}}^{\uparrow}$ against that estimated from CERES observations. Improvements to simulation of CCSM3-simulated $S_{\text{TOA}}^{\uparrow}$ by utilising MODIS-derived surface albedo are also examined. Three experiments considered a 10-year climate simulation using CCSM3 without any modification (CONTROL), constrained using MODIS observations of land surface characteristics

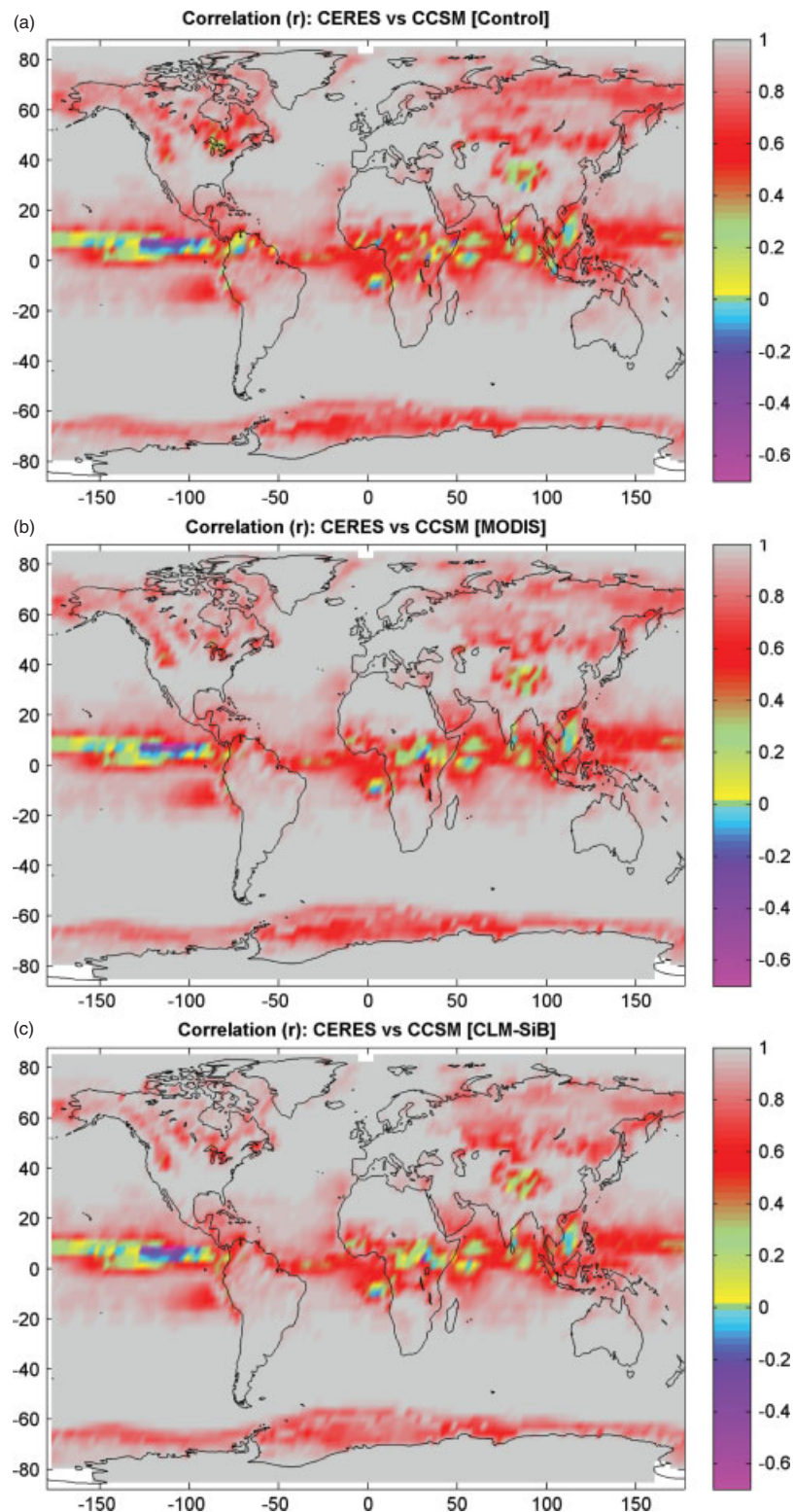


Figure 9. Correlation coefficient between monthly-averaged S_{TOA}^{\uparrow} from CERES observations and the CCSM3 experiments (a) CONTROL, (b) CLM-MODIS, and (c) CLM-SiB. This figure is available in colour online at wileyonlinelibrary.com/journal/joc

(CLM-MODIS), and CLM-MODIS in combination with the SiB hydrological model (CLM-SiB). The S_{TOA}^{\uparrow} from these three experiments was compared against a climatology of the same derived from CERES observations. Systematic biases in the CCSM3 radiative transfer parameterisation are examined using observations from

two ARM sites. The major findings from this study include

1. Comparison between CERES-observed and CCSM3-simulated S_{TOA}^{\uparrow} is complicated due to systematic over-estimation of transmissivity in the CAM3 radiative

transfer parameterisation. At selected sites, after accounting for this systematic bias, comparison to CERES observations shows that CCSM3-simulated $S_{\text{TOA}}^{\uparrow}$ improves when the MODIS-derived vegetation albedo and soil colour are used in CLM.

- Utilisation of MODIS albedo observations does not have a significant impact on the globally averaged value of $S_{\text{TOA}}^{\uparrow}$. However, it does have a significant seasonal impact when averaged over land areas and also at regional scales. Substantial improvements are found over the Sahara and Arabian Deserts and over agricultural regions. CCSM3 also overestimates $S_{\text{TOA}}^{\uparrow}$ over high altitude sites such as the Tibetan Plateau, presumably due to the inability to resolve the spatial heterogeneity of snow cover.
- CCSM3 generally underestimates $S_{\text{TOA}}^{\uparrow}$ over ocean areas, except over areas of sea ice and high wind speeds where it is overestimated. Correspondence between oceanic areas of high wind speeds and positive anomalies of $S_{\text{TOA}}^{\uparrow}$ is caused by the neglect of wind speed dependency in the parameterisation of OSA.
- CCSM3 substantially underestimates $S_{\text{TOA}}^{\uparrow}$ over the Saharan and Arabian Deserts and utilisation of MODIS-derived land surface albedo to constrain CCSM3 simulation improves simulation of $S_{\text{TOA}}^{\uparrow}$ over these regions.

This study shows that the TOA radiation budget in GCMs can be improved through the use of MODIS-derived land surface albedo. Use of MODIS-derived albedo improves the pattern of annual variation of the simulated $S_{\text{TOA}}^{\uparrow}$ and further improvement may be achieved through the use of the SiB land surface scheme. Analysis and elimination of systematic errors in the CCSM3 radiative transfer parameterisation are also needed to fully realise the advantage gained through the use of MODIS-derived albedo.

Acknowledgements

This research was sponsored by: the National Aeronautic and Space Administration via NNS06AA58G; the NOAA Office of Atmospheric Research Laboratories and Cooperative Institutes via NA06OAR4600181; and by the National Science Foundation via NSF ATM0437583 and NSF 0639838. CERES data were obtained from the NASA Langley Research Center Atmospheric Science Data Center. We are also grateful to the U.S. Department of Energy – Atmospheric Radiation Measurement Program for the *insitu* observations from the ARM instruments, and also to the European Central for Medium Range Forecasts for the ERA-40 dataset. We thank the two anonymous reviewers and Dr. Patrick Fitzpatrick for their helpful comments and suggestions to improve the manuscript. We are also grateful to Dallas Staley for her outstanding services in editing this manuscript.

References

- Bender FAM, Rodhe H, Charlson RJ, Ekman AML, Loeb N. 2006. 22 views of the global albedo – comparison between 20 GCMs and two satellites. *Tellus: Series A* **58**: 320–330, DOI: 10.1111/j.1600-0870.2006.00181.x.
- Bonan GB, Levis S, Kergoat L, Oleson KW. 2002. Landscapes as patches of plant functional types: an integrated concept for climate and ecosystem models. *Global Biogeochemical Cycles* **16**: 1021–1051, DOI: 10.1029/2000 GB001360.
- Cess RD, Potter GL, Gates WL, Morcrette J-J, Corsetti L. 1992. Comparison of general circulation models to Earth radiation budget experiment data: computation of clear-sky fluxes. *Journal of Geophysical Research* **97**: 20421–20426.
- Charlson RJ, Schwartz SE, Hales JM, Cess RD, Coakley JA Jr, Hansen JE, Hoffman DJ. 1992. Climate forcing by anthropogenic aerosols. *Science* **255**: 423–430, DOI: 10.1126/science.255.5043.423.
- Chen T, Rossow WB, Zhang Y-C. 2000. Radiative effects of cloud-type variations. *Journal of Climate* **13**: 264–286, DOI: 10.1175/1520-0442(2000)013<0264:REOCTV>2.0.CO;2.
- Dickinson RE, Oleson KW, Bonan GB, Hoffman F, Thornton PE, Vertenstein M, Yang ZL, Zeng X. 2006. The Community Land Model and its climate statistics as a component of the Community Climate System Model. *Journal of Climate* **19**: 2302–2324, DOI: 10.1175/JCLI3742.1.
- Dirmeyer PA, Gao X, Zha M, Guo Z, Oki T, Hanasaki N. 2005. The second Global Soil Wetness Project (GSWP-2): multi-model analysis and implications for our perception of the land surface. COLA Technical Report 185, 46 pp.
- Friedl M, McIver DK, Hodges JCF, Zhang XY, Muchoney D, Strahler AH, Woodcock CE, Gopal S, Schneider A, Cooper A, Baccini A, Gao F, Schaaf C. 2002. Global land cover mapping from MODIS: algorithms and early results. *Remote Sensing of the Environment* **83**: 287–302, DOI: 10.1016/S0034-4257(02)00078-0.
- Flanner MG, Zender CS. 2005. Snowpack radiative heating: influence on Tibetan plateau climate. *Geophysical Research Letters* **32**: L06501, DOI: 10.1029/2004GL022076.
- Hall A. 2004. The role of surface albedo feedback in climate. *Journal of Climate* **17**: 1550–1568, DOI: 10.1175/1520-0442(2004)017<1550:TROSAF>2.0.CO;2.
- Hansen MC, DeFries RS, Townshend JRG, Dimiceli C, Carroll M, Sohlberg R. 2003. Global percent tree cover at a spatial resolution of 500 meters: first results of the MODIS vegetation continuous fields algorithm. *Earth Interactions* **7**: 1–15, DOI: 10.1175/1087-3562(2003)007<0001:GPTCAA>2.0.CO;2.
- IPCC 2007. *Climate Change 2007: The Physical Science Basis*. Contribution of Working Group I to the Fourth Assessment Report of the Intergovernmental Panel on Climate Change. Solomon S, Qin D, Manning M, Chen Z, Marquis M, Averyt KB, Tignor M, Miller HL (eds.) Cambridge University Press: Cambridge, UK and New York, USA, 996 pp.
- Jin Z, Charlock TP, Smith WL Jr, Rutledge K. 2004. A parameterization of ocean surface albedo. *Geophysical Research Letters* **31**: L22301, DOI: 10.1029/2004GL021180.
- Kato S, Ackerman TP, Clothiaux EE, Mather JH, Mace GG, Wesely ML, Murcray F, Michalsky J. 1997. Uncertainties in modeled and measured clear-sky surface shortwave irradiances. *Journal of Geophysical Research* **102**: 25881–25898.
- Kinne S, Bergstrom R, Toon OB, Dutton E, Shiobara M. 1998. Clear-sky atmospheric solar transmission: an analysis based on FIRE 1991 field experiment data. *Journal of Geophysical Research* **103**: 19709–19720.
- Lawrence PJ, Chase TN. 2007. Representing a MODIS consistent land surface in the Community Land Model (CLM 3.0). *Journal of Geophysical Research* **112**: G01023, DOI: 10.1029/2006JG000168.
- Lawrence PJ, Chase TN. 2009. Climate impacts of making evapotranspiration in the Community Land Model (CLM3) consistent with the Simple Biosphere Model (SiB). *Journal of Hydrometeorology* **10**: 374, DOI: 10.1175/2008JHM987.1.
- Levis S, Bonan GB, Lawrence PJ. 2007. Present-day springtime high-latitude surface albedo as a predictor of simulated climate sensitivity. *Geophysical Research Letters* **34**: L17703, DOI: 10.1029/2007GL030775.
- Li J, Scinocca J, Lazare M, McFarlane N, von Salzen K, Solheim L. 2006. Ocean surface albedo and its impact on radiation balance in climate models. *Journal of Climate* **19**: 6314–6333, DOI: 10.1175/JCLI3973.1.

- Loeb NG, Kato S, Loukachine K, Manalo-Smith NM. 2005. Angular distribution models for top-of-atmosphere radiative flux estimation from the Clouds and the Earth's Radiant Energy System instrument on the Terra Satellite. Part I: Methodology. *Journal of Atmospheric and Oceanic Technology* **22**: 338–351, DOI: 10.1175/JTECH1712.1.
- Loeb NG, Kato S, Loukachine K, Manalo-Smith NM, Doelling DR. 2007. Angular distribution models for top-of-atmosphere radiative flux estimation from the clouds and the Earth's Radiant Energy System Instrument on the Terra satellite. Part II: Validation. *Journal of Atmospheric and Oceanic Technology* **24**: 564–584, DOI: 10.1175/JTECH1983.1.
- Myneni R, Hoffman S, Knyazikhin Y, Privette JL, Glassy J, Tian Y, Wang Y, Song X, Zhang Y, Smith GR, Lotsch A, Friedl M, Morisette JT, Votava P, Nemani RR, Running SW. 2002. Global products of vegetation leaf area and fraction absorbed PAR from year one of MODIS data. *Remote Sensing of the Environment* **83**: 214–231, DOI: 10.1007/978-3-540-37293-6_7.
- Nair US, Ray DK, Wang J, Christopher SA, Lyons TJ, Welch RM, Pielke RA Sr. 2007. Observational estimates of radiative forcing due to land use change in southwest Australia. *Journal of Geophysical Research* **112**: D09117, DOI: 10.1029/2006JD00750.
- Oleson KW, Bonan GB, Schaaf C, Gao F, Jin Y, Strahler A. 2003. Assessment of global climate model land surface albedo using MODIS data. *Geophysical Research Letters* **30**: 1443, DOI: 10.1029/2002GL016749.
- Oleson KW, Dai Y, Bonan G, Bosilovich M, Dickinson RE, Dirmeyer P, Hoffman F, Houser P, Levis S, Niu G, Thornton P, Vertenstein M, Yang Z-L, Zeng X. 2004. Technical description of the Community Land Model (CLM). NCAR Technical Note, NCAR/TN-461+STR, 173 pp.
- Patadia F, Yang E-S, Christopher SA. 2009. Does dust change the clear sky top of atmosphere shortwave flux over high surface reflectance regions?. *Geophysical Research Letters* **36**: L15825, DOI: 10.1029/2009GL039092.
- Potter GL, Cess RD. 2004. Testing the impact of clouds on the radiation budgets of 19 atmospheric general circulation models. *Journal of Geophysical Research* **109**: D02106, DOI:10.1029/2003JD004018.
- Qu X, Hall A. 2006. Assessing snow albedo feedback in simulated climate change. *Journal of Climate* **19**: 2617–2630, DOI: 10.1175/JCLI3750.1.
- Ramankutty N, Foley JA. 1999. Estimating historical changes in global land cover: croplands from 1700 to 1992. *Global Biogeochemical Cycles* **13**: 997–1027, 10.1046/j.1365-2699.1999.00141.x.
- Roesch A. 2006. Evaluation of surface albedo and snow cover in AR4 coupled climate models. *Geophysical Research Letters* **111**: D15111, DOI: 10.1029/2005JD006473.
- Schaaf CB, Gao F, Strahler AH, Lucht W, Li X, Tsang T, Strugnell NC, Zhang X, Jin Y, Muller J-P, Lewis P, Barnsley M, Hobson P, Disney M, Roberts G, Dunderdale M, Doll C, d'Entremont RP, Hu B, Liang S, Privette JL, Roy D. 2002. First operational BRDF, albedo nadir reflectance products from MODIS. *Remote Sensing of Environment* **83**: 135–148, DOI: 10.1016/S0034-4257(02)00091-3.
- Tarasova TA, Fomin BA. 2000. Solar radiation absorption due to water vapor: Advanced broadband parameterizations. *Journal of Applied Meteorology* **39**: 1947–1951, DOI: 10.1175/1520-0450(2000)039<1947:SRADTW>2.0.CO;2.
- Tarasova TA, Nobre CA, Holben BN, Eck TF, Setzer A. 1999. Assessment of smoke aerosol impact on surface solar irradiance measured in the Rondonia region of Brazil during Smoke, Clouds, and Radiation – Brazil. *Journal of Geophysical Research* **104**: 161–170.
- Tian Y, Dickinson RE, Zhou L, Myneni RB, Friedl M, Schaaf CB, Carroll M, Gao F. 2004a. Land boundary conditions from MODIS data and consequences for the albedo of a climate model. *Geophysical Research Letters* **31**: L05504, DOI: 10.1029/2003GL019104.
- Tian Y, Dickinson RE, Zhou L, Shaikh M. 2004b. Impact of new land boundary conditions from Moderate Resolution Imaging Spectroradiometer (MODIS) data on the climatology of land surface variables. *Journal of Geophysical Research* **109**: D20115, DOI: 10.1029/2003JD004499.
- Wang Z, Zeng X, Barlage M. 2007. Moderate Resolution Imaging Spectroradiometer bidirectional reflectance distribution function-based albedo parameterization for weather and climate models. *Journal of Geophysical Research* **112**: D02103, DOI:10.1029/2005JD006736.
- Wang Z, Zeng X, Barlage M, Dickinson RE, Gao F, Schaaf CB. 2004. Using MODIS BRDF and albedo data to evaluate global model land surface albedo. *Journal of Hydrometeorology* **5**: 3–14, DOI: 10.1175/1525-7541(2004)005<0003:UMBAAAD>2.0.CO;2.
- Wild M. 2008. Short-wave and long-wave surface radiation budgets in GCM: a review based on IPCC-AR4/CMIP3 models. *Tellus* **60A**: 932–945, DOI: 10.1111/j.1600-0870.2008.00342.x.
- Wild M, Ohmura A, Gilgen H, Roeckner E. 1995. Validation of general circulation model radiative fluxes using surface observations. *Journal of Climate* **8**: 1309–1324.
- Zhou L, Dickinson RE, Tian Y, Zeng X, Dai Y, Yang Z, Schaaf CB, Gao F, Jin Y, Strahler A, Myneni RB, Yu H, Wu W, Shaikh M. 2003. Comparison of seasonal and spatial variations of albedos from Moderate-Resolution Imaging Spectroradiometer (MODIS) and Common Land Model. *Journal of Geophysical Research* **108**(D15): 4488, DOI:10.1029/2002JD003326.